Cite this: DOI: 10.1039/xxxxxxxxxx

Hydrogel-colloid interfacial interactions: a study of tailored adhesion using optical tweezers

Amir Sheikhi[a‡] and Reghan J. Hill[a*]

Received Date
Accepted Date

DOI: 10.1039/xxxxxxxxxx

www.rsc.org/journalname

Dynamics of colloidal particles adhering to soft, deformable substrates, such as tissues, biofilms, and hydrogels play a key role in many biological and biomimetic processes. These processes, including, but not limited to colloid-based delivery, stitching, and sorting, involve microspheres exploring the vicinity of soft, sticky materials in which the colloidal dynamics are affected by the fluid environment (*e.g.*, viscous coupling), inter-molecular interactions between the colloids and substrate (*e.g.*, Derjaguin-Landau-Verwey-Overbeek (DLVO) theory), and viscoelastic properties of the contact region. To better understand colloidal dynamics at soft interfaces, an optical tweezers back-focal-plane interferometry apparatus was developed to register the transverse Brownian motion of a silica microsphere in the vicinity of polyacrylamide (PA) hydrogel films. The time-dependent mean-squared displacement is well described by a single exponential relaxation, furnishing measures of the transverse interfacial diffusion coefficient and binding stiffness. Substrates with different elasticities were prepared by changing the PA crosslinking density, and the inter-molecular interactions were adjusted by coating the microspheres with fluid membranes. Stiffer PA hydrogels (with bulk Young's moduli ≈ 1–10 kPa) immobilize the microspheres more firmly (lower diffusion coefficient and position variance), and coating the particles with zwitterionic lipid bilayers completely eliminates adhesion, possibly by attractive dispersion forces. Remarkably, embedding polyethylene glycol-grafted lipid bilayers (DSPE-PEG2k-Amine) in the zwitterionic fluid membranes produces stronger adhesion, possibly because of polymer-hydrogel attraction and entanglement. This study provides new insights to guide the design of nanoparticles and substrates with tunable adhesion, leading to smarter delivery, sorting, and screening of micro- and nanosystems.

1 Introduction

Colloidal and polymer adhesion to soft, deformable substrates is of fundamental and practical importance to drug delivery,[1–3] biomedical[4–8] and microfluidic[9–11] sciences (*e.g.*, micro- and nano-patterning, and cell capture and sorting), environmental engineering,[12–14] and biology.[15] Silica particle-based drug delivery has gained tremendous attention within the past decade owing to thermal and chemical stability, and stealth properties.[16–18] To achieve smart drug delivery, precise control over the colloidal particle-tissue adhesion dynamics is required for directing drug carriers toward affected organs. A large portion of such carriers, for example in rat intravenous delivery, may become trapped in lung and liver tissue when the particles are larger than ≈ 300 nm.[16]

Natural entrapment of colloids occurs in a wide range of biological processes. Immobilization of therapeutic agents by endothelia or their engulfment through phagocytosis are some important examples.[19,20] Salps, a pelagic tunicate, despite having a large mesh size, use a soft, sticky net under a laminar flow to trap and filter sub-micron particles.[21] Another intriguing case arises from recent efforts to design micro- and nano-carriers to penetrate or adhere to mucus for drug delivery.[2,22,23] Although many experimental observations have been conducted, little is known about how particles behave upon contact with soft substrates. The model system adopted in this work to study rigid-body interactions with a soft substrates comprises a silica microsphere on a thin hydrogel film.

Hydrogels, as hydrophilic polymer networks that can absorb water up to thousands times of their dry weight,[24] have been introduced as model systems for biological tissues and extracellular matrices.[25–28] Tunable elasticity provides a platform for studying the effect of substrate stiffness on cell attachment,[29] migration,[30]

[a] Department of Chemical Engineering, McGill University, 3610 University Street, Montreal, Quebec, H3A 0C5, Canada. Fax: +1 514 398 6897; Tel: +1 514 398 6678; E-mail: reghan.hill@mcgill.ca

‡ Present address: Department of Chemistry, McGill University. E-mail: amir.sheikhi@mail.mcgill.ca

This journal is © The Royal Society of Chemistry [year]

secretion,[31] differentiation,[32,33] and shape.[34] Polyacrylamide hydrogel surfaces with customizable elasticity have been used to accommodate and regulate a top-sitting species,[35–38] and owing to their excellent transparency (at low enough PA concentrations), optical techniques are readily implemented.

On length and time scales relevant to micron-sized particles, such interfaces are subject to hydrodynamic draining and deformation, which impact kinetic and thermodynamic adhesion factors.[39] Recently, soft adhesion dynamics have been studied theoretically for a bare colloidal particle and a polymer-coated rigid substrate.[39,40] Such adhesion can adopt a stepwise mechanism initiated with long-bond formation between the surfaces, followed by short-bond establishment.[39] Recent experiments involving an interacting colloidal probe with a rigid glass substrate show that a bare silica particle undergoes a rapid immobilization upon contact at high (low) ionic strength (restoring force and/or oscillatory shear rate), whereas a soft polystyrene bead adheres gradually to a stiff substrate.[41–44] Such phenomena are hypothesized to be related to the time-dependent formation of bonds between the soft particle and the rigid substrate.

Combining colloidal particles with soft hydrogels has attracted recent attention for modifying gels[45] and characterizing them,[46] sorting particles in microarrays,[47] inducing colloid-colloid attraction,[48] mimicking drug delivery[49] and bioadhesion,[50] and performing wet adhesion.[51], as reviewed by Thoniyot *et al.*[52] Despite extensive experimental studies of soft adhesion at an air interface (reviewed by Sheikhi[53]), wet adhesion at aqueous interfaces is unexplored.

In this work, optical tweezers back-focal-plane interferometry is applied to conduct passive microrheology for quantifying colloidal particle-hydrogel interfacial adhesion. Brownian fluctuations of an optically-trapped silica microsphere at positions close to and when attached to a hydrated polyacrylamide film are registered. The goal is to understand how particle dynamics are affected by functional coatings and substrate viscoelastic properties.

2 Materials and methods

2.1 Hydrogel preparation

For each experiment, a thin layer of PA hydrogel was covalently adhered to a glass cover slip according to the literature.[54] Square cover glasses (22×22 mm, thickness No. 1, Fisher Scientific, ON, Canada) were cleaned by 30 min boiling in 7X solution (MP Biomedical, Solon, OH, U.S.A.) followed by reverse osmosis (RO) water rinses. These were dried under nitrogen and immersed in a freshly-prepared piranha solution (3:1 v/v concentrated sulfuric acid and 30 % hydrogen peroxide) for 20 min. Etched cover glasses were extensively rinsed with RO water, dried under nitrogen, and allowed to contact 0.5 mol L^{-1} sodium hydroxide solution followed by a silanization agent (3-aminopropyltrimethoxysilane, 97 %, Sigma-Aldrich, MO, U.S.A.) with intermediate gentle rinses in RO water. Finally, the cover glasses were incubated in 0.7 % glutaraldehyde (70 % EM Grade, Polysciences, Inc., PA, U.S.A.) with phosphate buffered saline (PBS, pH ≈ 7.4) at room temperature for 30 min, and then rinsed thoroughly with RO water. The pre-gel solution for the stiffest hydrogel (A) was prepared by mixing ≈ 5 % w/v acrylamide solution diluted with PBS from a 40% w/v stock solution of 19:1 w/w acrylamide to bis-acrylamide crosslinker (Fisher BioReagents, NJ, U.S.A.) resulting in a final crosslinker concentration ≈ 0.25 % w/v, and the semi-stiff (B) and soft (C) hydrogels were made by manually mixing and diluting an acrylamide solution (40 % w/v) with bis-acrylamide solution (2 % w/v) in PBS buffer to final mixtures comprising 5 % w/v acrylamide and 0.15 % w/v bis-acrylamide (33.3:1 w/w acrylamide to bis-acrylamide) and 0.049 % w/v bis-acrylamide (102:1 w/w acrylamide to bis-acrylamide), respectively. The solutions were purged with nitrogen to prevent oxygen absorption during crosslinking. The gel was formed by sandwiching $\lesssim 1$ μL of pre-gel solution between the functionalized cover glass and a cleaned (and non-functionalized) cover glass followed by an ≈ 10 min cure with ≈ 0.001% w/v ammonium persulfate (APS, Sigma-Aldrich, MO, U.S.A.) initiator and 0.1% v/v N,N,N′,N′-tetramethylethylenediamine (TEMED, GE Healthcare, Uppsala, Sweden). To achieve an equilibrium swollen state, the thin film was incubated in tris-acetate-EDTA (TAE, pH ≈ 8.3 with 40 mmol L^{-1} ionic strength tris-acetate and 1 mmol L^{-1} EDTA, Sigma, MO, U.S.A.) buffer for at least one day at the ambient temperature ($\approx 23^{\circ}$C), followed by rinsing with the buffer. The bulk rheological properties of these gels, measured by small amplitude oscillatory shear (SAOS) furnish steady storage moduli $G'_{t\to\infty} \approx 3617$, 2080, and 414 Pa for gels A, B, and C, respectively (Electronic Supplementary Information). The stiffnesses of hydrogels A, B, and C[55,56] mimic the elasticity of human thyroid/mouse skeletal muscle, human breast tumor/guinea pig lung, and human liver, respectively.[57] The surface potentials of PA hydrogels were characterized using an electrokinetic analyzer (Anton Paar, Graz, Austria) mounted with an asymmetric clamping cell, and in general accordance with literature.[58]

2.2 Colloidal particle preparation

Bare silica microspheres (diameter ≈ 1.97 μm, 10–15% coefficient of variation, Bangs Laboratories, Inc., IN, U.S.A.) were cleaned using at least two centrifugations in TAE buffer. These were injected into a custom-built sealed channel including the gel-coated cover glass (150–200 μm thick, bottom), glass microscope slide (≈ 1 mm thick, top), and millimeter-thick plexiglas spacer (shown in figure 1) at a particle concentration 40 μL^{-1}. To coat microspheres with bilayers, small unilamellar vesicles (SUV) were prepared following the literature.[59] Briefly, a phospholipid mixture containing 2 mg 1,2-dioleoyl-sn-glycero-3-phosphocholine (DOPC, Avanti Polar Lipids, Alabaster, AL, U.S.A.) and a favored lipopolymer 1,2-distearoyl-sn-glycero-3-phosphoethanolamine-N-[amino(polyethylene glycol)2000] (DSPE-PEG2k-Amine, Avanti Polar Lipids, Alabaster, AL, U.S.A.) concentration (0 and 2.5 mol%) in chloroform was dried under nitrogen. This was desiccated under vacuum for at least 1 h followed by reconstitution in PBS buffer (pH = 7.4) to 2 mg mL^{-1}. The resulting giant multilamellar vesicles (GMV) were extruded through 100 nm and 50 nm polycarbonate membranes (Avanti Polar Lipids, Alabaster, AL, U.S.A.) each at least 20 times, respectively, to assemble SUVs, which were stored in a fridge (4°C) and used within a

This journal is © The Royal Society of Chemistry [year]

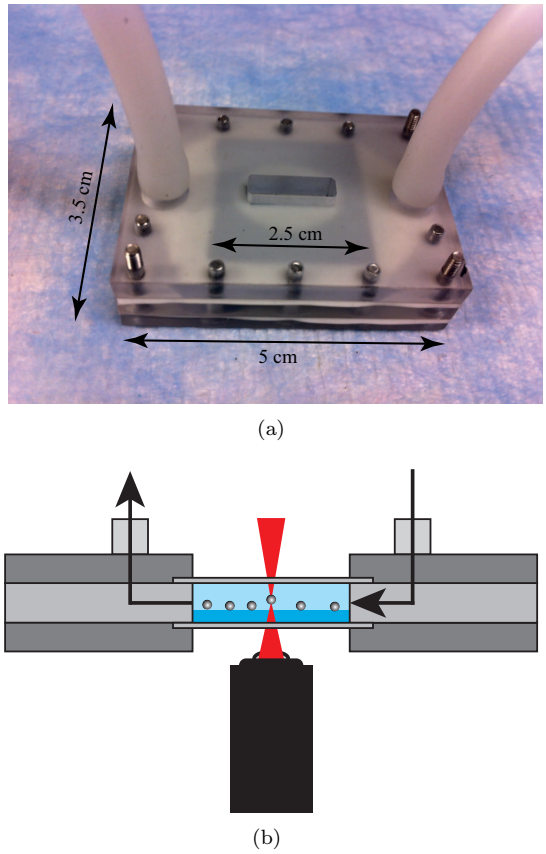

Fig. 1 Custom-built flow cell (a) and schematic (not to scale) (b). Colloidal microspheres in buffer solution are injected into the chamber, and one particle is trapped using optical tweezers at various heights $z \lesssim 1$ μm above the hydrogel interface ($z = 0$), using a nano-positioning stage; the glass microscope slide (top) and a hydrogel-coated cover glass (bottom) are separated by a plexiglas spacer.

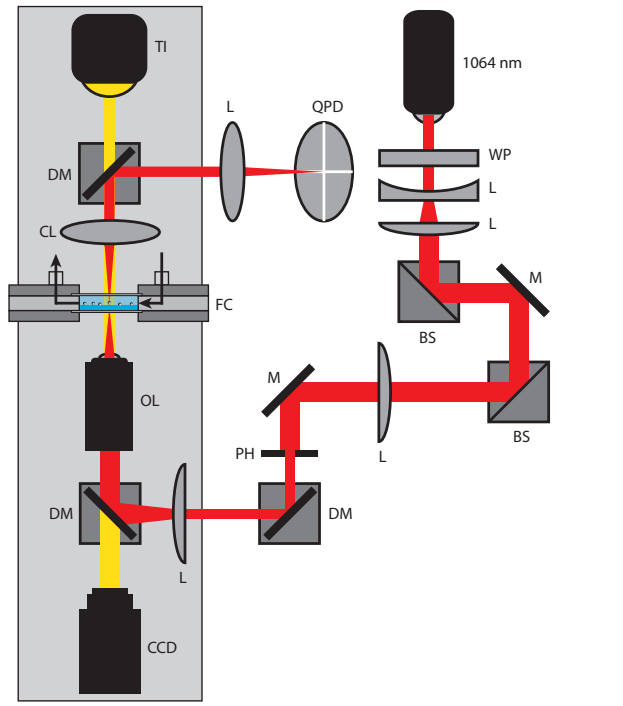

Fig. 2 Optical tweezers interfacial microrheology schematic: 1064 nm ND-YVO_4 laser, lenses (L), condenser lens (CL), half waveplate (WP), pinhole (PH), polarizing beam splitters (BS), beam dump (BD), mirrors (M), dichroic mirrors (DM), CCD camera, high numerical aperture objective lens (OL), flow cell (FC) mounted on a piezoelectric nanopositioning stage, quadrant photodiode detector (QPD), and tungsten illuminator (TI). Components not associated the optical tweezers operation are shown within the box on the left.

few hours. To coat silica microspheres with lipid bilayers, spheres were mixed with the SUV solution[60] at a particle (10 w%):lipid ratio 1:3 v/v and stirred for at least 10 min. To eliminate infused SUVs,[60] the particle-lipid mixture was pulse-centrifuged and the supernatant was separated followed by dilution in TAE buffer at least three times. Coated particles were diluted in TAE buffer (pH = 8.3). The particle ζ-potentials were measured using a Zetasizer Nano ZS instrument (Malvern Instruments, UK).

2.3 Optical tweezers

A single colloidal microsphere is trapped using a custom-built optical tweezers instrument,[61] shown schematically in figure 2. This comprises a steerable high-power 1064 nm ND-YVO_4 laser (BL-106C, Spectra-Physics, U.S.A.) collimated and directed through the high numerical aperture (NA) 100X objective lens of an inverted optical microscope (TE-2000U, Nikon, NY, U.S.A.). The sample (figure 1) is translated vertically using a nano-positioning stage (NPXYZ100B, nPoint, WI, U.S.A.) in 20 nm increments, and the optically-trapped microsphere position fluctuations are recorded using back-focal-plane interferometry, whereby transmitted and scattered light is directed through the microscope condenser lens onto a quadrant photodiode detector (QPD, Spot-9dmi, OSI Optoelectronics, CA, U.S.A.). QPD voltage time series are amplified using a dual-axis position-sensing amplifier (501C, UDT Instruments, CA, U.S.A.) and filtered at 10 kHz (half the sampling frequency) for 10 s time periods. These time series are proportional to the particle displacement from the centre of the optical trap, and were calibrated to ascertain the trap stiffness and voltage-to-displacement scaling factor using power spectrum analysis.[62] The calibration procedure is detailed elsewhere.[53] A 3D feed-back control system was implemented to eliminate particle-position offset from the trap centre following particle adhesion.[53] In this work, we measure only the lateral position fluctuations of optically trapped microspheres, because the vertical particle position variances upon contact with the gel are smaller than the instrument detection limit. The gel-electrolyte interface is identified (approximately) by an abrupt change (decrease) in the particle position time-series. Under these conditions, images of an optically trapped particle are the same as those of other particles on the gel. Because no interfacial gel deformation could be seen, any deformation likely occurs with displacements below optical resolution.

3 Results and discussion

Three types of colloidal probes, namely bare silica, phospholipid bilayer (DOPC)-coated silica, and lipopolymer (DSPE-PEG2k-Amine)-doped phospholipid bilayer-coated silica microspheres

were optically trapped and brought into contact with PA hydrogels A, B, and C. A schematic of these materials is presented in figure 3.

3.1 Bare silica microspheres

Bare microsphere position time series $X(t)$ are shown in figure 4, from which the mean-squared displacement $\langle[X(t+\tau)-X(t)]^2\rangle$ versus time lag τ is directly computed and shown in figure 5 with accompanying fits to the two-parameter model:[63]

$$\langle[X(t+\tau)-X(t)]^2\rangle = 2\langle X^2\rangle[1-\exp(-\tau D_x/\langle X^2\rangle)], \qquad (1)$$

where D_x is the lateral diffusion coefficient and $\langle X^2\rangle$ is the variance. From the Stokes-Einstein relationship and equipartition theorem, $D_x = k_BT/\gamma_x$ and $\langle X^2\rangle = k_BT/k_x$, where k_BT is the thermal energy, γ_x is the friction coefficient, and k_x is the spring constant.

Under conditions where the particle is trapped far from a cover glass or gel, $\gamma_x \to 6\pi\eta R$ and $k_x \to k_{x,t}$, where $k_{x,t}$ is the optical trap spring constant. Accordingly, fitting Eqn. (1) to the data in figure 5 with distance from the cover glass $h \approx 20$ μm furnishes $D_x \approx 0.24$ μm^2 s^{-1} and $\langle X^2\rangle \approx 370$ nm^2, giving $2R = \gamma_x/(3\pi\eta) \approx 2$ μm and $k_x \approx k_{x,t} \approx 11$ μN m^{-1}, which are both in good agreement with the values from the power-spectrum analysis.

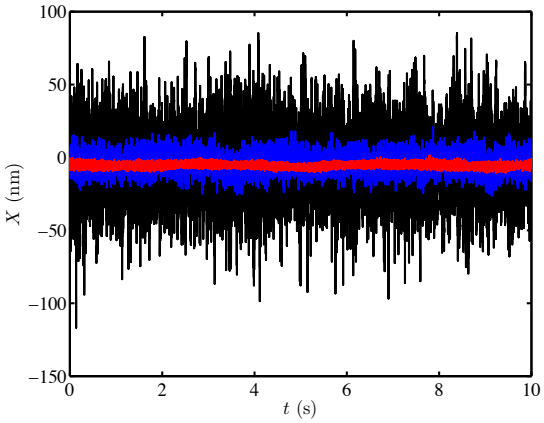

Fig. 4 Time series of the lateral particle position fluctuations $X(t)$ of an optically trapped silica microsphere (diameter $2R \approx 1.97$ μm) at height ≈ 20 μm from the bottom wall of a gel-free channel (black), on a polyacrylamide gel A (blue), and immobilized on a cover glass at physiological ionic strength after one day of equilibration (red). The voltage-to-position scale factor and optical trap spring constant for an elevated and attached particle are furnished by the power spectrum and attached-particle calibration methods, respectively.[53]

Next, assuming that $k_{x,t}$ and α are independent of the trap height z (relative to the gel surface) over the range of heights in experiments with particles interacting with a gel ($z \lesssim 1$ μm, figure 1b), D_x and $\langle X^2\rangle$ are obtained at various positions z above the apparent hydrogel-electrolyte interface. As the particle is brought closer to the interface, coupling to the gel attenuates D_x and $\langle X^2\rangle$, and particle contact can be identified by a discontinuous change in D_x and $\langle X^2\rangle$ over a distance that is less than the ≈ 20 nm vertical displacement increment of the nanopositioning stage. Once the particle attaches to the gel, k_x ($\langle X^2\rangle$) increases (decreases) substantially, because the particle dynamics become dominated by coupling to the gel, which overwhelms the optical force. Accordingly, the data in figure 5 with a particle attached to the gel A (blue symbols) furnish $D_x \approx 0.014$ μm^2 s^{-1} and $\langle X^2\rangle \approx 31$ nm^2 following attachment.

Dynamics of a bare silica particle in the vicinity of hydrogels A, B, and C are shown in figure 6 as a height/time-dependent diffusion coefficient (left panel) and position variance as an indicator of binding stiffness (right panel) for an elevated/adhered particle. Particle ($z > 0$) diffusion coefficients decrease when approaching the substrate because of hydrodynamic friction. The data are compared with Faxen[64] (blue), O'Neill[65] (green) and Goldman *et al.*[66] (red) theories. Given an almost-constant trap stiffness with such a small gap, attenuation of the diffusion coefficient can be attributed to the hydrodynamic interaction with the substrate. Although the hydrogel is soft and porous with 95 % bound water, it behaves hydrodynamically as a rigid barrier. Linear short-time behavior of the mean-squared displacement (see figure 5) suggests no anomalous diffusion when near and attached to the gels.

Once the particle adheres to the hydrogel, its diffusion coefficient undergoes an abrupt decrease, reflecting a strong lubrication or viscous drag. Attenuation from contact with the substrate is greater for the stiffest hydrogel (gel A), which reduces the diffusion coefficient to 5 % of the bulk value, whereas softer hydrogels B and C reduce the equilibrium short-time diffusion coefficient to ≈ 10 % of the bulk value. The attenuation occurs abruptly for hydrogels A and B, suggesting that adhesive bond formation between the particle and the interface is spontaneous and that the bonds are similar in length and stickiness. To understand the origin of the attraction, the ζ-potentials of the bare silica microspheres in TAE buffer, and streaming potentials of PA gel-coated cover glasses were measured. Oppositely-signed potentials for silica microspheres ($\zeta \approx -52$ mV) and a gel-coated slide (streaming potential in TAE buffer, 27 mV) induce charge attraction, which is enhanced at small particle-gel separations (*e.g.*, $z \lesssim 10$ nm) by dispersion forces. Note that the positive charge of PA in TAE buffer must be attributed to buffer-cation adsorption. When the same gels were tested in 4.1 and 41 mmol L^{-1} NaCl solutions, the PA streaming potentials were only ≈ 4.3 and ≈ 0 mV, respectively, whereas in TAE buffer containing 41 mmol L^{-1} NaCl, the PA streaming potential was ≈ 21.5 mV.

The softest gel C, with five-fold lower crosslinker concentration than gel A, has a much lower crosslinking density, and thus a larger mesh size. Upon contact with gel C, as presented in figure 6(c), the diffusion coefficient (left panel) and position variance (right panel) of the bare colloidal probe decrease gradually with time, suggesting a gradual adhesion, similar to the modelled adhesion of a colloidal particle to a polymer-coated surface.[39] This indicates a gradual penetration of the colloidal microsphere into the gel on an ≈ 1500 s time scale. Similar behavior has been reported for a sticking transition of a (soft) polystyrene microsphere on a rigid glass substrate.[41] According to this study, when the interacting bodies are rigid (a silica microsphere on a rigid glass substrate), no 'aging' is observed.

The position fluctuation variance reflects the binding stiffness; the lower the variance, the stiffer is the potential in which the particle is trapped. As the gel height varies slightly from one ex-

This journal is © The Royal Society of Chemistry [year]

periment to another, the optical trap stiffness, which affects the particle position variance in the bulk electrolyte, varies. Thus, by calibrating the trap before each experiment, the variance is normalized, yielding an average value $k_{x,t}/k_{x,t}(z \gtrsim 1\ \mu\text{m}) \approx 1$ for an elevated particle (figure 6, right panel, when $z > 0$). Once the particle is trapped at the hydrogel interface, the position variance decreases, furnishing $\langle X^2 \rangle^{1/2} \approx 5$, 6.4, and 9.2 nm for the stiff (A), semi-stiff (B), and soft (C) gels, respectively. For the softest gel, the variance decreases approximately exponentially, thus reflecting time-dependent binding. Note that the probe particle position variances are inversely related to the bulk shear moduli. For particles fully embedded in these gels, the position variances are typically lower than the instrument detection limit; optical tweezers microrheology is feasible only when the elastic modulus is about one order of magnitude lower than in this study.[67]

The foregoing experiments were repeated with randomly selected bare silica microspheres on different gel surfaces, and the position variance and diffusion coefficients are presented in figure 7. The differences from repeated experiments show how hydrogels arrest the particle motion. Depending on the local gel properties, *e.g.*, nano-scale roughness and surface wrinkles, the particles undergo different dynamics; however, on average, as can be seen in figure 7 (right panel), the short-time diffusion coefficient decreases with increasing substrate stiffness. The position variance also decreases when increasing the substrate stiffness (as seen in figure 7, left panel), indicating that a stiff substrate slows the dynamics more than a soft one. This might be of particular interest for guiding the design of micro- and nano-fluidic devices for particle rolling, separation, and sorting.

3.2 Phospholipid bilayer-coated microspheres

We modified the interfacial dynamics by altering the electrostatic and dispersion (van der Waals) forces between the microsphere and the substrate, *i.e.*, by changing the surface potential and effective Hamaker constant. Bare silica microspheres were coated with zwitterionic lipid bilayers (DOPC), which reduced the ζ-potential from ≈ -52 mV for bare spheres to ≈ -30 mV. Note that the addition of DSPE-PEG2k-Amine did not impart a significant change in the particle ζ-potential. These lipopolymers displace the positive quaternary charge of DOPC to the terminal primary amine-functionalized PEG2k ends, but do not change the net charge, which is zero. Thus, electro-osmotic flow in the peripheral region, driven by the terminal amine, is compensated by an oppositely directed inner electro-osmotic flow due to the negative dialkyl phosphate moiety.

This is in accordance with literature: e.g., a decrease in ζ-potential from ≈ -60 mV to ≈ -25 mV at pH ≈ 8 and 5 mmol L^{-1} KCl following the addition of 1 mg DOPC/100 mL to 10 mg bare silica particles has been reported.[68]

The lateral diffusion coefficient and position variance are presented in figure 8. Interestingly, regardless of the substrate stiffness, bilayer coatings promote free diffusion. With $z \approx 40$ nm, a DOPC-coated particle adopts $D_x/D_0 \approx 0.45$, which theoretically corresponds to $z \approx 100$ nm. Such a high diffusion coefficient is unchanged after adhering to the gel, suggesting that the bilayer coating maintains an effective particle-hydrogel separation ≈ 100 nm.

Thus, decreasing the Hamaker constant seems to explain the enhanced repulsion. The Hamaker constant for silica and acrylamide interacting through water $A_{s-w-a} \approx (\varepsilon_s - \varepsilon_w)(\varepsilon_a - \varepsilon_w)/[(\varepsilon_s + \varepsilon_w)(\varepsilon_a + \varepsilon_w)] \approx 10^{-20}$ J[69], so the Hamaker constant for DOPC-water-acrylamide is lower by a factor $A_{b-w-a}/A_{s-w-a} \approx (\varepsilon_b - \varepsilon_w)(\varepsilon_s + \varepsilon_w)/[(\varepsilon_s - \varepsilon_w)(\varepsilon_b + \varepsilon_w)] \approx -1.105(\varepsilon_b - 80)/(\varepsilon_b + 80) \approx 0.31$ (evaluated using an effective DOPC dielectric constant $\varepsilon_b \approx 45$,[70] $\varepsilon_w \approx 80$, and $\varepsilon_s \approx 4$[71]), evidently preventing the attachment of dangling PA chains to the bilayer-coated microspheres. Note that the foregoing reduction of the Hamaker constant can even lead to a net repulsive dispersion force when $\varepsilon_b \gtrsim 80$. This is possible because the effective dielectric constant for DOPC can be higher than for water, as demonstrated experimentally by Zhuo *et al.*[72], owing to its zwitterionic head groups.

We also probed the surface texture of the gels by moving the optically-trapped bilayer-coated particles along the interface, but observed no significant surface undulation. This non-adhesive system provides an ideal platform to study the interactions between embedded moieties in the bilayers, such as polymer chains and hydrogels. In the next section, we examine grafted-polymer-hydrogel interfacial interactions.

3.3 Lipopolymer-doped bilayer-coated microspheres

Given that DOPC bilayers produce a repulsive interaction, we doped the bilayers with polyethylene glycol (PEG, $M_w = 2000$) chains using DSPE-PEG2k-Amine to shed light on the polymer-hydrogel interfacial interaction. Such particles have been used in drug delivery to enhance blood-circulation relative to bare or lipid-coated silica particles.[73]

Figure 9 presents the lateral diffusion coefficient and position variance of a lipopolymer (DSPE-PEG2k-Amine, 2.5 mol%)-doped DOPC-coated silica microsphere in the contact vicinity of PA hydrogels A and B. At this concentration, PEG chains are close to the brush regime.[74] When an optically-trapped particle is in the bulk electrolyte, its Brownian diffusion closely follows the continuum hydrodynamic models, as shown by solid lines in figure 9 (left panels). Upon contact with PA hydrogels, particles strongly adhere to the hydrogel. Optical restoring forces with spring constants as large as $\approx 40\ \mu\text{N m}^{-1}$ were unable to detach these particles. Such adhesion seems to reflect the interaction of the grafted polymer chains with the hydrogel surface, since zwitterionic bilayers without polymer did not adhere (figure 8).

It is possible that the interaction with gel the disturbs the bilayer coating, possibly exposing patches of bare silica to PA. However, this seems unlikely as these particles did not exhibit the slow adhesive dynamics we observed for bare silica interacting with the softest gels. The ζ-potentials of DOPC-coated and DSPE-PEG2k-Amine-doped DOPC-coated microspheres are similar (≈ -30 mV), suggesting that electrostatic interactions play a weak role in the adhesion. Thus, assuming that the bilayers remain intact, we speculate that the attraction arises between PEG and PA. Since PEG chains can penetrate and, therefore, entangle with the PA network, without the significant entropic penalty required to compress a brush at an impenetrable interface, the par-

Table 1 Colloidal probe position variances $\langle X^2 \rangle$ (nm^2) from figures 6, 8, and 9 upon contact with PA hydrogel films A ($G'_{t\to\infty} \approx 3617$ Pa), B ($G'_{t\to\infty} \approx 2080$ Pa), and C ($G'_{t\to\infty} \approx 414$ Pa).

Silica microsphere coating	$\langle X^2 \rangle_A$	$\langle X^2 \rangle_B$	$\langle X^2 \rangle_C$
Bare	25	41	85
DOPC	–	–	–
DSPE-PEG2k-Amine	60	80	–

ticles are likely to position themselves in an energy minimum that is dominated by the van der Waals repulsive interaction between DOPC and the gel, and an intrinsic attraction between PEG and PA. Such a configuration would impart a much weaker interfacial disruption of the gels than suggested by the adhesion of bare silica particles to the softest gel C. This is supported, in part, by the much larger particle position variances for DSPE-PEG2k-Amine-doped DOPC-coated microspheres when attached to the gels, as elaborated upon below.

Average values (over several different particles at different positions) of the particle position variance and lateral diffusion coefficient are shown in figure 10. While diffusion is similar for hydrogels A and B (left panels), the position variance (right panels) with the softer gel (B) is slightly higher than for hydrogel A (similarly to bare particles, softer gels produce weaker adhesion). For both gels, the diffusion coefficient and position variance are significantly higher than for their bare counterparts.

A summary of particle position variances is presented in Table 1. For gels A, B, and C, respectively, the effective crosslinking densities $n_{t\to\infty} = G'_{t\to\infty}/k_BT \approx 8.85\times10^5$, 5.09×10^5, and 1.01×10^5 μm^{-3}, which correspond to mesh sizes $\xi \approx 10$, 13, and 21 nm (all $\ll R$). The crosslinker-to-monomer ratios (mol/mol) are $\approx 2.4\%$, 1.4%, and 0.4%, corresponding to ideal shear moduli $G' = nk_BT \approx 39900$, 22800, and 7440 Pa. These furnish crosslinking efficiencies $G'_{t\to\infty}/G'_{ideal} \approx 9$, 9, and 5.6%, for gels A, B, and C, respectively. Here, n is the crosslinker number density. The low efficiencies attest to a large number of dangling and looped chains, which do not contribute to the network elasticity.

Finally, the maximum number of PEG chains that could interact with the gel may be estimated as follows. First, assuming that the PEG-grafting density in the contact region equals the particle average, the DSPE-PEG2k-Amine grafting density $\Gamma_l = x/A_l$, where the mole fraction of DSPE-PEG2k-Amine in DOPC $x \approx 0.025$ and the average area of a lipid $A_l \approx 0.6$–0.7 nm^2.[75] Next, the area within a circle where the normal separation between the particle and a perfectly flat gel is less than a distance l is $A_p \approx 2\pi Rl$, where $R \gg l$ is the particle radius. It follows that the number of DSPE-PEG2k-Amine molecules in this contact region $N_p = A_p\Gamma_l \approx 2\pi Rlx/A_l$. Note the l cannot exceed the PEG2k chain contour length $l_c \approx 16$ nm,[76] so the maximum number of chains in the contact region $N_p \approx 4{,}200$. On the other hand, if l is taken to be the PEG2k Flory radius $R_F \approx 3.5$ nm,[77,78] then the maximum number of chains in the contact region may be $N_p \approx 920$. Note that lipids are able to diffuse within the bilayer coating (fluid membrane), which may concentrate chains in the contact region when the average concentration is less than the mushroom-to-brush transition concentration. Estimates of this transition concentration vary in the literature from about 2 to 4%,[74,79,80] and is otherwise considered to occur gradually.[59] Nevertheless, assuming an adhesive interaction energy per PEG2k chain $\sim k_BT$, the maximum force required to separate the surfaces is $\sim k_BTN_p/l \sim 1$ nN, which is about two orders of magnitude greater than typical optical trapping forces.

4 Conclusions

Soft interfacial inclusions occur in a wide range of biological systems, where a relatively stiff agent, such as a colloidal carrier, meets a soft organ/cell. To understand how the substrate stiffness and particle surface influence the interactions, single silica microsphere dynamics were registered when particles are bought into close contact with a polyacrylamide (PA) hydrogel. We showed that PA hydrogels firmly hinder the bare-particle dynamics: the stiffer the hydrogel, the stiffer the interfacial binding. Sticky microparticles were then converted to non-adhesive particles by coating with a zwitterionic (DOPC) lipid bilayer membrane. Thus, particle adhesion could be significantly influenced/tuned via the the van der Waals contribution to the DLVO interaction, rather than by adjusting the net surface charge. We then introduced polyethylene glycol-conjugated lipid bilayers (DSPE-PEG2k-Amine in DOPC) as coatings to probe the interaction between grafted polymer chains and a hydrogel. The nano-sized PEG chains formed strong bridges between micron-sized particles and hydrogels, evidently overcoming the repulsive DLVO potential that prevailed without PEGylation. This research provides insights into interfacial properties of soft inclusions, which may be helpful for designing smart soft coatings for advanced drug delivery, micro- and nano-separation, and high-throughput sorting/screening devices.

5 Acknowledgments

The authors acknowledge support from a Natural Sciences and Engineering Research Council of Canada (NSERC) Discovery Grant (R.J.H.), the Canada Research Chairs (CRC) program (R.J.H), a McGill Engineering Doctoral Award (A.S.), and the Center for Self Assembled Chemical Structures. A.S. thanks Dr. J. van Heiningen, McGill University, Prof. E. Eiser and T. Yanagishima, Cambridge University, Prof. K. Berg-Sørensen, Technical University of Denmark, and Prof. S. Jeney and M. Grimm, Ecole Polytechnique Federale de Lausanne (EPFL) for helpful discussions. Thanks to Prof. N. Tufenkji, McGill University for use of Electrokinetic Analyzer and Zetasizer instruments.

References

1 Y.-Y. Wang, S. Lai, C. So, C. Schneider, R. Cone and J. Hanes, *PLoS ONE*, 2011, **6**, e21547.

2 L. Ensign, C. Schneider, J. Suk, R. Cone and J. Hanes, *Adv. Mater.*, 2012, **24**, 3887–3894.

3 B. E. B. Jensen, L. Hosta-Rigau, P. R. Spycher, E. Reimhult, B. Stadler and A. N. Zelikin, *Nanoscale*, 2013, **5**, 6758–6766.

4 S. Lai, Y.-Y. Wang, K. Hida, R. Cone and J. Hanes, *Proc. Natl. Acad. Sci. U.S.A.*, 2010, **107**, 598–603.

5 E. Nance, G. Woodworth, K. Sailor, T.-Y. Shih, Q. Xu,

This journal is © The Royal Society of Chemistry [year]

G. Swaminathan, D. Xiang, C. Eberhart and J. Hanes, *Sci. Transl. Med.*, 2012, **4**, 149ra119.
6 T.-Y. Cheng, H.-C. Wu, M.-Y. Huang, W.-H. Chang, C.-H. Lee and T.-W. Wang, *Nanoscale*, 2013, **5**, 2734–2744.
7 B. M. Teo, L. Hosta-Rigau, M. E. Lynge and B. Stadler, *Nanoscale*, 2014, **6**, 6426–6433.
8 J. Lu, F. Zheng, Y. Cheng, H. Ding, Y. Zhao and Z. Gu, *Nanoscale*, 2014, **6**, 10650–10656.
9 O. Usta, M. Nayhouse, A. Alexeev and A. Balazs, *J. Chem. Phys.*, 2008, **128**, 235102–1–235102–8.
10 P. Liu, J. Sun, J. Huang, R. Peng, J. Tang and J. Ding, *Nanoscale*, 2010, **2**, 122–127.
11 Q. Yu, L. K. Ista, R. Gu, S. Zauscher and G. P. Lopez, *Nanoscale*, 2016, **8**, 680–700.
12 C. Leon-Morales, A. Leis, M. Strathmann and H.-C. Flemming, *Water Res.*, 2004, **38**, 3614–3626.
13 S. Tripathi, D. Champagne and N. Tufenkji, *Environ. Sci. Technol.*, 2012, **46**, 6942–6949.
14 R. Li, L. Zhang and P. Wang, *Nanoscale*, 2015, **7**, 17167–17194.
15 M. Lamblet, B. Delord, L. Johannes, D. van Effenterre and P. Bassereau, *Eur. Phys. J. E*, 2008, **26**, 205–216.
16 C. Barbe, J. Bartlett, L. Kong, K. Finnie, H. Lin, M. Larkin, S. Calleja, A. Bush and G. Calleja, *Adv. Mater.*, 2004, **16**, 1959–1966.
17 D. Knopp, D. Tang and R. Niessner, *Anal. Chim. Acta*, 2009, **647**, 14 – 30.
18 T. Yu, A. Malugin and H. Ghandehari, *ACS Nano*, 2011, **5**, 5717–5728.
19 M. Herant, V. Heinrich and M. Dembo, *Journal of cell science*, 2006, **119**, 1903–1913.
20 R. E. Serda, J. Gu, J. K. Burks, K. Ferrari, C. Ferrari and M. Ferrari, *Cytometry Part A*, 2009, **75**, 752–760.
21 K. Sutherland, L. Madin and R. Stocker, *Proc. Natl. Acad. Sci. U.S.A.*, 2010, **107**, 15129–15134.
22 B. Schuster, J. Suk, G. Woodworth and J. Hanes, *Biomaterials*, 2013, **34**, 3439–3446.
23 S. Md, G. Singh, A. Ahuja, R. Khar, S. Baboota, J. Sahni and J. Ali, *Systematic Reviews in Pharmacy*, 2012, **3**, 4–14.
24 A. S. Hoffman, *Adv. Drug Delivery Rev.*, 2002, **54**, 3 – 12.
25 Y.-E. Ju, P. Janmey, M. McCormick, E. Sawyer and L. Flanagan, *Biomaterials*, 2007, **28**, 2097–2108.
26 A. L. Plant, K. Bhadriraju, T. A. Spurlin and J. T. Elliott, *Biochim. Biophys. Acta, Mol. Cell. Res.*, 2009, **1793**, 893 – 902.
27 J. Reed, W. Walczak, O. Petzold and J. Gimzewski, *Langmuir*, 2009, **25**, 36–39.
28 M. J. Choi, S. R. Guntur, K. I. Lee, D. G. Paeng and A. Coleman, *Ultrasound in Medicine & Biology*, 2013, **39**, 439 – 448.
29 R. Sunyer, A. Jin, R. Nossal and D. Sackett, *PLoS ONE*, 2012, **7**, e46107.
30 M. Ng, A. Besser, G. Danuser and J. Brugge, *J. Cell Biol.*, 2012, **199**, 545–563.
31 A. Petersen, P. Joly, C. Bergmann, G. Korus and G. Duda, *Tissue Engineering - Part A*, 2012, **18**, 1804–1817.
32 J. Liu, Y. Tan, H. Zhang, Y. Zhang, P. Xu, J. Chen, Y.-C. Poh, K. Tang, N. Wang and B. Huang, *Nat. Mater.*, 2012, **11**, 734–741.
33 N. Eroshenko, R. Ramachandran, V. Yadavalli and R. Rao, *Journal of Biological Engineering*, 2013, **7**, 1–8.
34 S.-Y. Tee, J. Fu, C. Chen and P. Janmey, *Biophys. J.*, 2011, **100**, L25–L27.
35 T. Ulrich, E. De Juan Pardo and S. Kumar, *Cancer Research*, 2009, **69**, 4167–4174.
36 P. Moshayedi, L. Da F Costa, A. Christ, S. Lacour, J. Fawcett, J. Guck and K. Franze, *J. Phys. Condens Matter*, 2010, **22**, 194114.
37 S. Sant, M. Hancock, J. Donnelly, D. Iyer and A. Khademhosseini, *Can. J. Chem. Eng.*, 2010, **88**, 899–911.
38 S. Ghosh, K. Ashcraft, M. Jahid, C. April, C. Ghajar, J. Ruan, H. Wang, M. Foster, D. Hughes, A. Ramirez, T. Huang, J.-B. Fan, Y. Hu and R. Li, *Nat. Commun.*, 2013, **4**, 1821.
39 M. Mani, A. Gopinath and L. Mahadevan, *Phys. Rev. Lett.*, 2012, **108**, 226104.
40 A. Gopinath and L. Mahadevan, *Proc. R. Soc. A*, 2011, **467**, 1665–1685.
41 P. Sharma, S. Ghosh and S. Bhattacharya, *Nat. Phys.*, 2008, **4**, 960–966.
42 P. Sharma, S. Ghosh and S. Bhattacharya, *Applied Phys. Lett.*, 2010, **97**, 104101–1–104101–3.
43 P. Sharma, S. Ghosh and S. Bhattacharya, *J. Chem. Phys.*, 2010, **133**, 144909.
44 D. Kumar, S. Ghosh and S. Bhattacharya, *J. Chem. Phys.*, 2012, **137**, 224901.
45 J. Yang, L.-H. Deng, C.-R. Han, J.-F. Duan, M.-G. Ma, X.-M. Zhang, F. Xu and R.-C. Sun, *Soft Matter*, 2013, **9**, 1220–1230.
46 P. S. Bhosale, J. Chun and J. C. Berg, *Langmuir*, 2011, **27**, 7376–7379.
47 M. Suzuki, T. Yasukawa, H. Shiku and T. Matsue, *Langmuir*, 2007, **23**, 4088–4094.
48 L. Di Michele, T. Yanagishima, A. Brewer, J. Kotar, E. Eiser and S. Fraden, *Phys. Rev. Lett.*, 2011, **107**, 136101.
49 O. Lieleg, I. Vladescu and K. Ribbeck, *Biophys. J.*, 2010, **98**, 1782–1789.
50 H. Takeuchi, H. Yamamoto and Y. Kawashima, *Adv. Drug Delivery Rev.*, 2001, **47**, 39–54.
51 S. Rose, A. Prevoteau, P. Elziere, D. Hourdet, A. Marcellan and L. Leibler, *Nature*, 2014, **505**, 382–385.
52 P. Thoniyot, M. J. Tan, A. A. Karim, D. J. Young and X. J. Loh, *Advanced Science*, 2015, **2**, n/a–n/a.
53 A. Sheikhi, *PhD thesis*, McGill University, 2015.
54 Y. Wang and J. R. Pelham, *Methods Enzymol.*, 1998, **298**, 489–496.
55 J. Tse and A. Engler, *Current Protocols in Cell Biology*, 2010, 10.16.1–10.16.16.
56 A. Engler, L. Bacakova, C. Newman, A. Hategan, M. Griffin and D. Discher, *Biophys. J.*, 2004, **86**, 617–628.

57 I. Levental, P. Georges and P. Janmey, *Soft Matter*, 2007, **3**, 299–306.

58 S. Walker, S. Bhattacharjee, E. Hoek and M. Elimelech, *Langmuir*, 2002, **18**, 2193–2198.

59 H.-Y. Zhang and R. Hill, *J. R. Soc. Interface*, 2011, **8**, 127–143.

60 M. Baksh, M. Jaros and J. Groves, *Nature*, 2004, **427**, 139–141.

61 J. A. van Heiningen, A. Mohammadi and R. J. Hill, *Lab Chip*, 2010, **10**, 1907–1921.

62 K. Berg-Srensen and H. Flyvbjerg, *Rev. Sci. Instrum.*, 2004, **75**, 594–612.

63 H. Clercx and P. Schram, *Phys. Rev. A*, 1992, **46**, 1942–1950.

64 H. Faxen, *Ark. Mat. Astron. Fys.*, 1923, **18**, 1–28.

65 M. E. O'Neill, *Mathematika*, 1964, **11**, 67–74.

66 A. Goldman, R. Cox and H. Brenner, *Chem. Eng. Sci.*, 1967, **22**, 637–651.

67 A. Mohammadi, *PhD thesis*, McGill University, 2011.

68 E. Chibowski, A. Delgado, K. Rudzka, A. Szcześ and L. Hołysz, *J. Colloid Interface Sci.*, 2011, **353**, 281–289.

69 L. Di Michele, A. Zaccone and E. Eiser, *Proc. Natl. Acad. Sci. U.S.A.*, 2012, **109**, 10187–10192.

70 A. Lomize, I. Pogozheva and H. Mosberg, *J. Chem. Inf. Model.*, 2011, **51**, 930–946.

71 J. Valle-Delgado, J. Molina-Bolivar, F. Galisteo-Gonzalez, M. Galvez-Ruiz, A. Feiler and M. Rutland, *J. Chem. Phys.*, 2005, **123**, 034708–1–034708–12.

72 K. Zhuo, Y. Chen, L. Kang, S. Xu and J. Wang, *Journal of Chemical & Engineering Data*, 2009, **54**, 137–141.

73 M. Van Schooneveld, E. Vucic, R. Koole, Y. Zhou, J. Stocks, D. Cormode, C. Tang, R. Gordon, K. Nicolay, A. Meijerink, Z. Fayad and W. Mulder, *Nano Letters*, 2008, **8**, 2517–2525.

74 D. Noppl-Simson and D. Needham, *Biophys. J.*, 1996, **70**, 1391–1401.

75 J. F. Nagle and S. Tristram-Nagle, *Current Opinion in Structural Biology*, 2000, **10**, 474 – 480.

76 N. Steinmetz and M. Manchester, *Biomacromolecules*, 2009, **10**, 784–792.

77 N. Efremova, B. Bondurant, D. O'Brien and D. Leckband, *Biochemistry*, 2000, **39**, 3441–3451.

78 N. Moore and T. Kuhl, *Langmuir*, 2006, **22**, 8485–8491.

79 A. Kenworthy, K. Hristova, D. Needham and T. McIntosh, *Biophysical Journal*, 1995, **68**, 1921–1936.

80 N. D. Santos, C. Allen, A.-M. Doppen, M. Anantha, K. A. Cox, R. C. Gallagher, G. Karlsson, K. Edwards, G. Kenner, L. Samuels, M. S. Webb and M. B. Bally, *Biochimica et Biophysica Acta (BBA) - Biomembranes*, 2007, **1768**, 1367 – 1377.

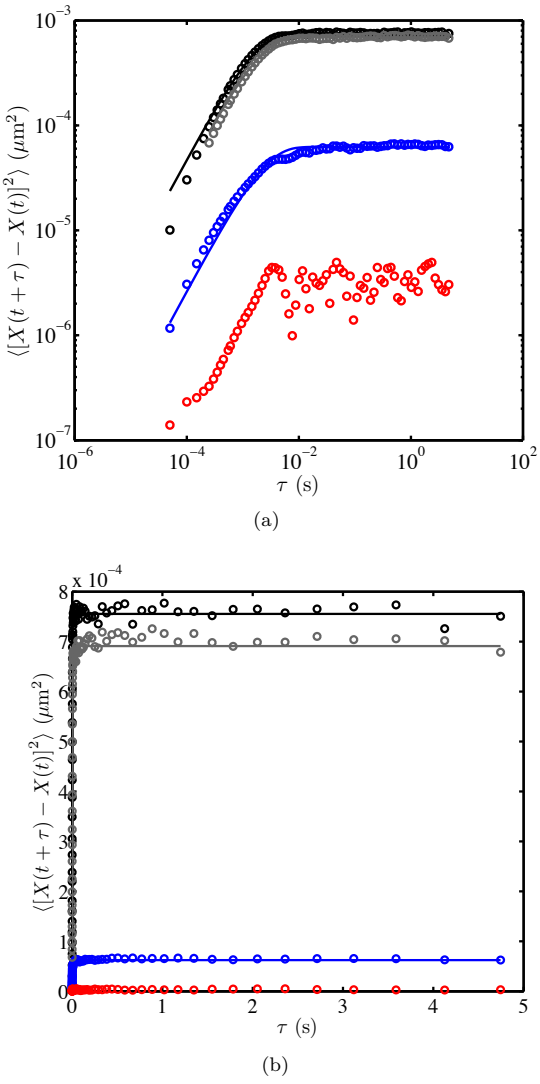

Fig. 5 Mean-squared displacement $\langle [X(t+\tau)-X(t)]^2 \rangle$ of bare silica microspheres in a gel-free channel (black), gel-coated channel (grey), when attached to a PA gel A film (blue), and while immobilized on a cover glass (red) at physiological ionic strength after one day of equilibration. The corresponding time series are presented in figure 4. Fitting Eqn. (1) to the data furnishes $D_x \approx 0.24$ μm^2 s^{-1} and $\langle X^2 \rangle \approx 370$ nm^2 (black); $D_x \approx 0.178$ μm^2 s^{-1} and $\langle X^2 \rangle \approx 346$ nm^2 (grey); and $D_x \approx 0.014$ μm^2 s^{-1} and $\langle X^2 \rangle \approx 31$ nm^2 (blue). Note the logarithmic and linearly scaled axes in panels (a) and (b), respectively.

This journal is © The Royal Society of Chemistry [year]

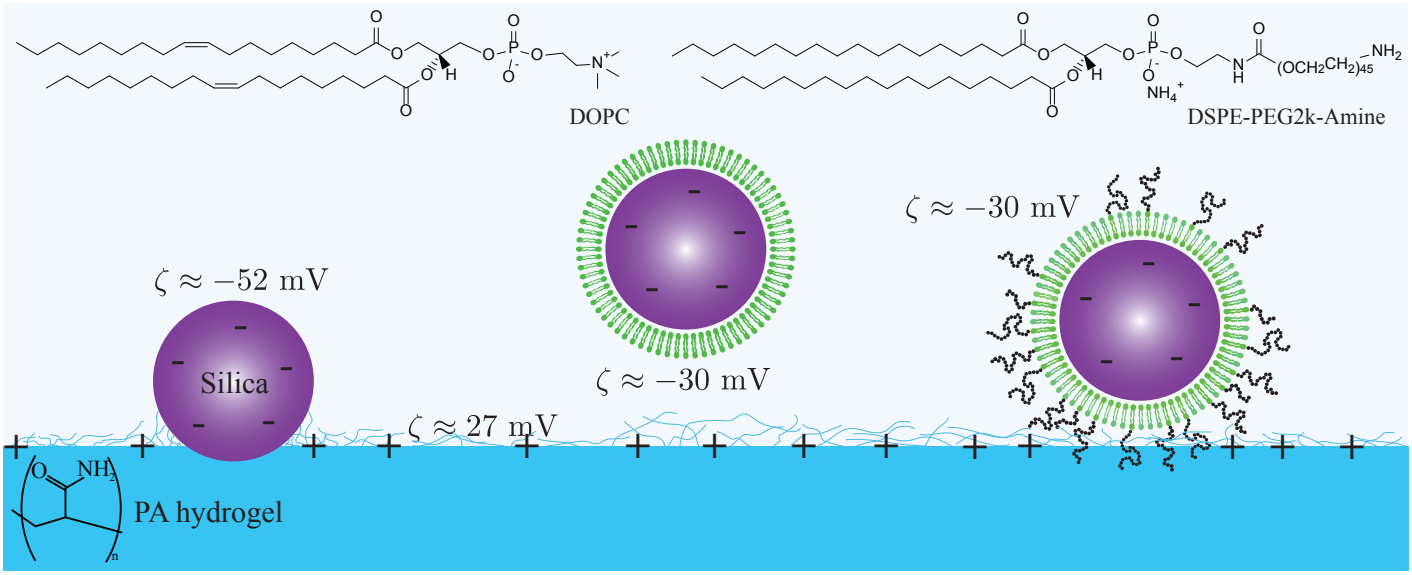

Fig. 3 Schematics of bare, DOPC-coated, and DSPE-PEG2k-Amine-doped DOPC-coated silica microspheres in the vicinity of a polyacrylamide (PA) hydrogel film. The chemical structure of the phospholipid bilayers (DOPC) and PEG-grafted bilayers (DSPE-PEG2k-Amine) are adapted from the vendor (Avanti Polar Lipids). For clarity, DSPE-PEG2k-Amine is only shown on the outer leaflet.

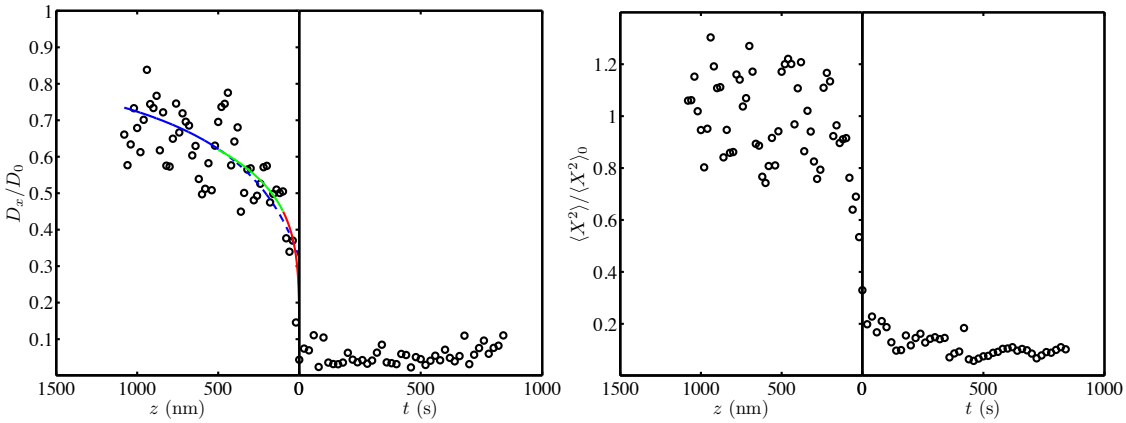

(a) Bare silica microsphere on PA hydrogel A

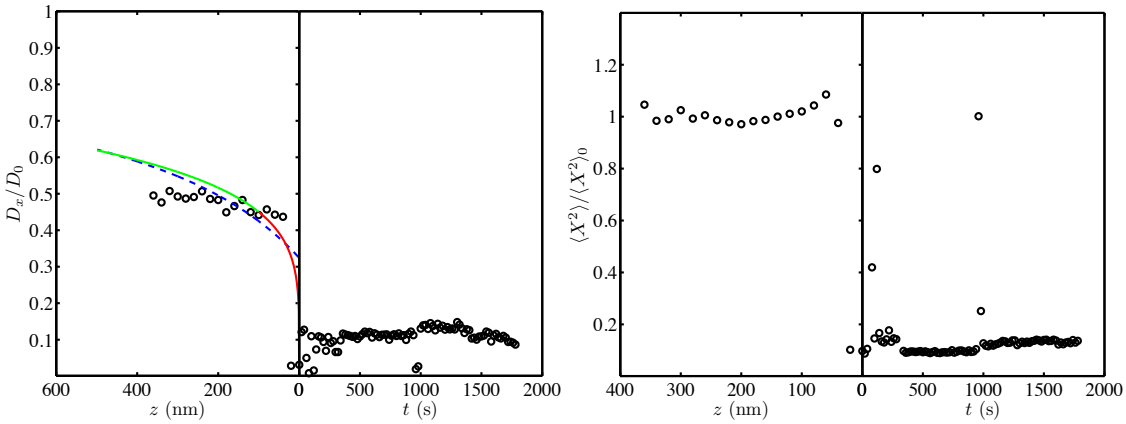

(b) Bare silica microsphere on PA hydrogel B

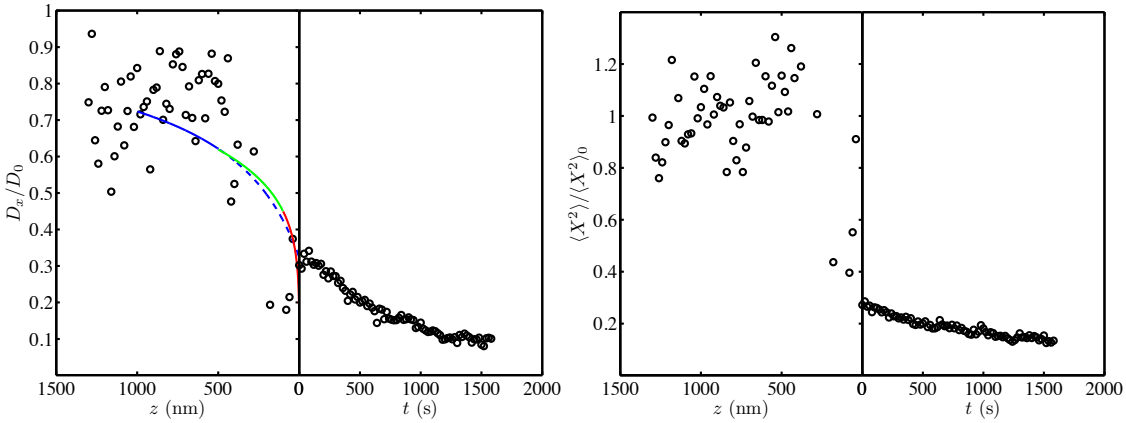

(c) Bare silica microsphere on PA hydrogel C

Fig. 6 Short-time diffusion coefficient (left panel) and long-time position variance (right panel) obtained from passive interfacial microrheology with optical tweezers and back-focal-plane interferometry position detection employing a bare silica microsphere on the surface of the stiff PA hydrogel A (panel a), semi-stiff PA hydrogel B (panel b), and soft PA hydrogel C (panel c). The particle ($2R \approx 1.97$ μm) is brought into contact with PA hydrogels by vertically translating the sample in 20 nm increments using a nano-positioning stage. The diffusion coefficients D_x (left panel) and the (long-time) variance of the transverse Brownian position fluctuations $\langle X^2 \rangle$ (right panel) are plotted versus the particle-hydrogel gap height z and time t when the particle is elevated and when it adheres to the interface, respectively. Lines in the left panel are the Faxen [64] (solid and dashed, blue), O'Neill [65] (green), and Goldman *et al.* [66] (red) hydrodynamic theories for the translation of a sphere parallel to a plane wall. Note that $\langle X^2 \rangle$ and D_x were obtained by fitting a single exponential relaxation to plots of $\langle [X(t+\tau) - X(t)]^2 \rangle$ versus the time lag τ: $D_0 \approx 0.25$ μm^2 s^{-1} and $\langle X^2 \rangle_0 \approx 350$ (panel a), 520 (panel b), and 780 nm^2 (panel c). These furnish equilibrium $\langle X^2 \rangle^{1/2} \approx 5$, 6.4, and 9.2 nm for the stiff (A), semi-stiff (B), and soft (C) gels, respectively.

This journal is © The Royal Society of Chemistry [year]

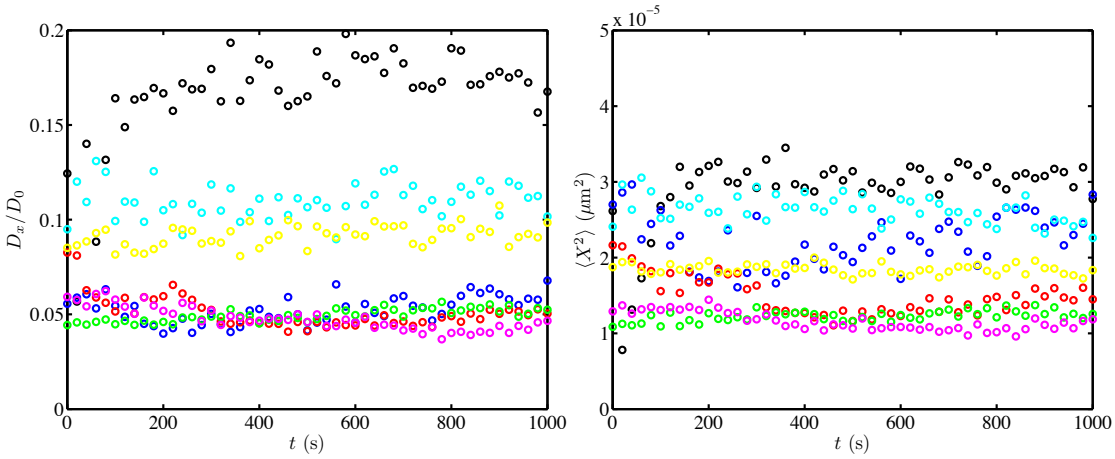

(a) Bare silica microspheres on PA hydrogel A

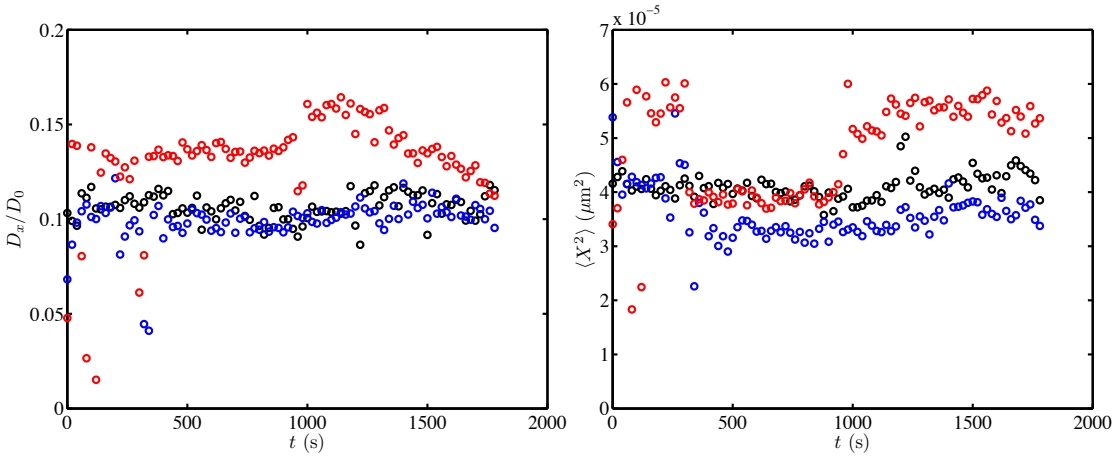

(b) Bare silica microspheres on PA hydrogel B

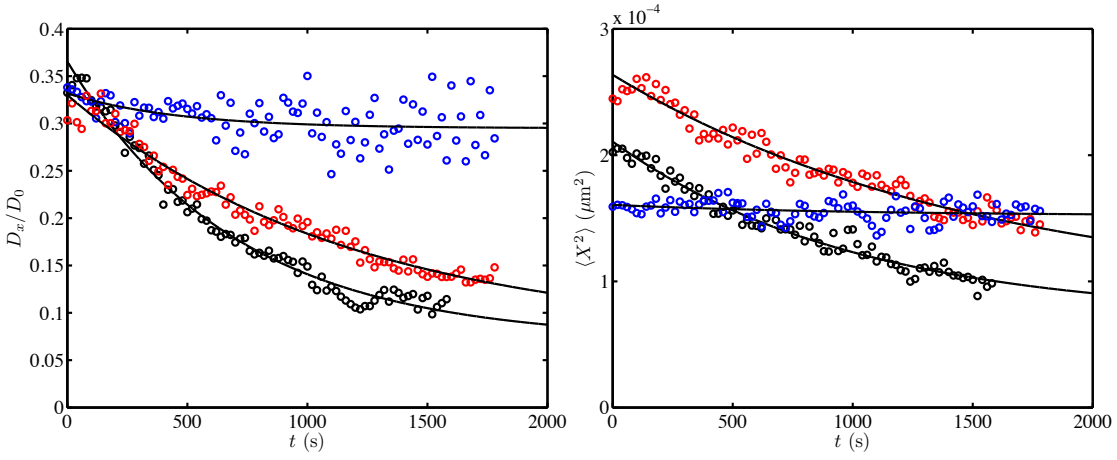

(c) Bare silica microspheres on PA hydrogel C

Fig. 7 Short-time diffusion coefficient (left panel) and long-time position fluctuation variance (right panel) of bare silica microspheres on various hydrogels. In the case of 'aging' with time (gel C), a single relaxation fit $C_1 + C_2 \exp(-t/\tau)$ (black lines) furnishes equilibrium values C_1. The position variance coefficients C_1, C_2, and τ are 88.4 nm^2, 175.3 nm^2, 1510 s (red symbols), 71.4 nm^2, 139.4 nm^2, and 1010 s (black symbols), and 152 nm^2, 8.6 nm^2, and 1000 s (blue symbols), respectively, furnishing equilibrium position variances 88.4, 71.4, and 152 nm^2, respectively. The diffusion coefficient fit parameters C_1, C_2, and τ are 0.075, 0.255, and 1171 s (red symbols), 0.071, 0.295, and 695 s with $R^2 \approx 0.98$ (black symbols), and 0.294, 0.037, and 456 s (blue symbols), respectively, furnishing equilibrium $D_x/D_0 \approx 0.075$, 0.071, and 0.29, respectively. Fitting Eqn. (1) to the data is undertaken with $\tau \lesssim 0.05$ s for gels A and B, and $\lesssim 0.1$ s for gel C, to avoid long-time drift artifacts. Colors identify properties acquired from one experiment on each gel.

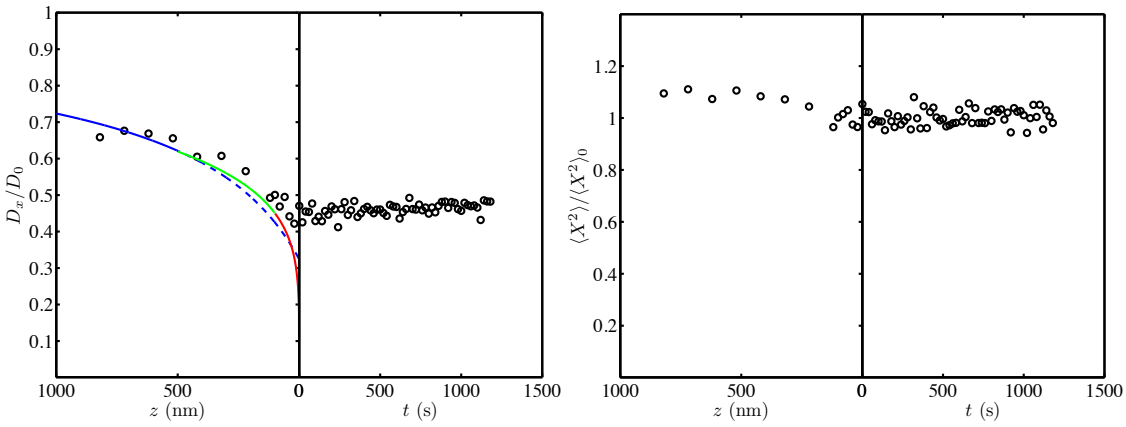

(a) DOPC-coated silica microsphere on PA hydrogel A

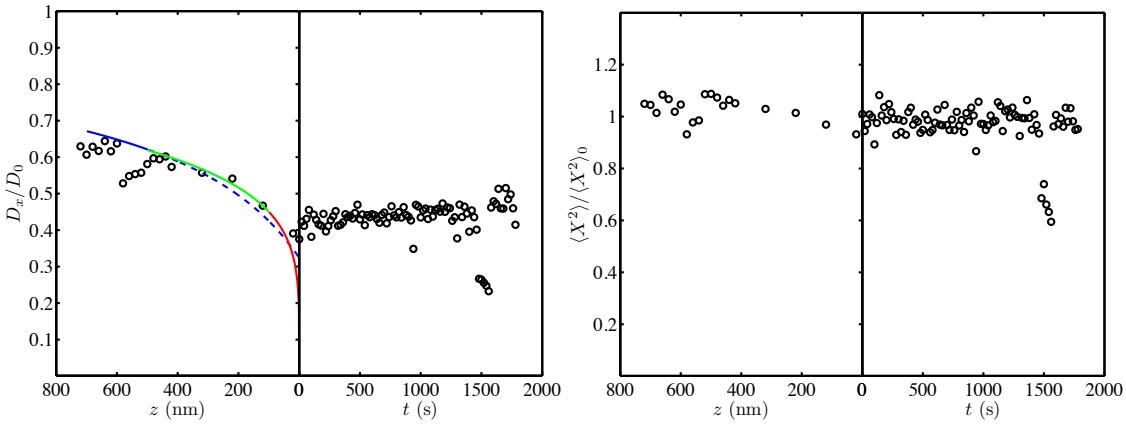

(b) DOPC-coated silica microsphere on PA hydrogel B

Fig. 8 Lateral diffusion coefficient (left panels) and position variance (right panels) of a DOPC-coated silica microsphere in the vicinity of PA hydrogels A (a) and B (b). This coating repels the probe from the hydrogel-electrolyte interface regardless of the gel stiffness. Here, contact with the soft substrates has no significant effect on the short-time diffusion coefficient or position variance. In right-panel figures a and b, $\langle X^2\rangle \approx \langle X^2\rangle_0 \approx 493$ and 531 nm, respectively, corresponding to the optical trap spring constant. The solid lines are theories detailed in figure 6.

This journal is © The Royal Society of Chemistry [year]

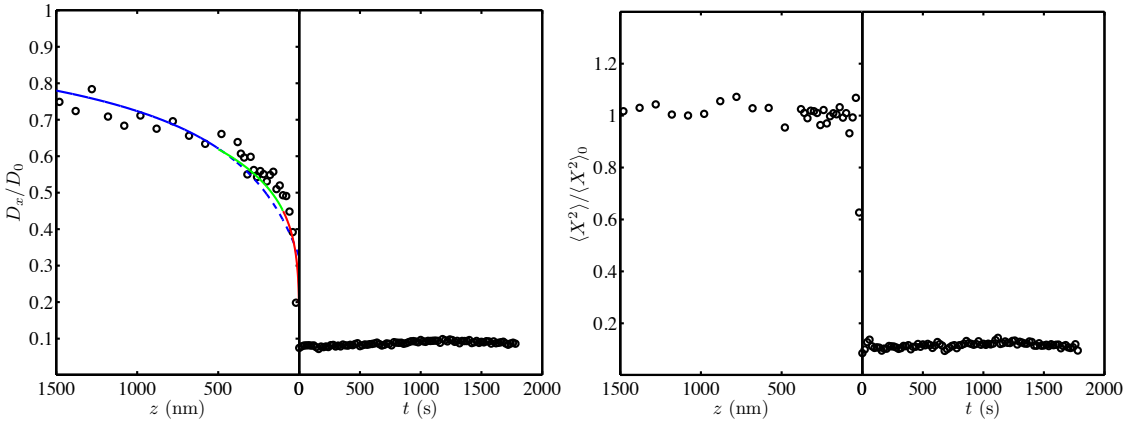

(a) DSPE-PEG2k-Amine/DOPC-coated silica microsphere on PA hydrogel A

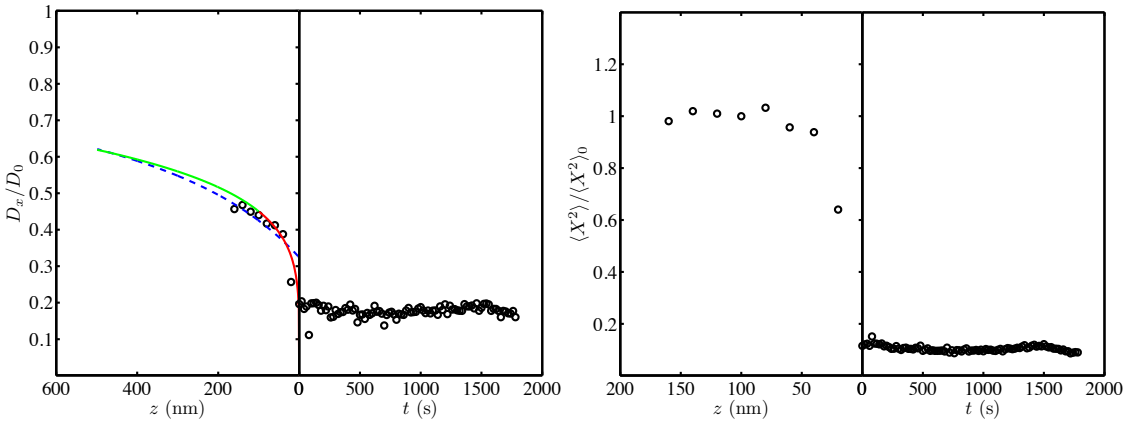

(b) DSPE-PEG2k-Amine/DOPC-coated silica microsphere on PA hydrogel B

Fig. 9 Passive interfacial microrheology with optical tweezers and back-focal-plane interferometry position detection for a polymer (DSPE-PEG2k-Amine, 2.5 mol%)-doped DOPC-coated silica microsphere ($2R \approx 1.97$ μm) brought into contact with polyacrylamide hydrogels A (a) and B (b) by vertically translating the sample in 20 nm increments using a piezo-electric nano-positioning stage. Dimensionless diffusion coefficients D_x/D_0 (left panels) and the (long time) variance of the transverse Brownian position fluctuations $\langle X^2 \rangle$ (right panels) are plotted versus the particle-hydrogel gap height z, and versus time t once the particle adheres to the interface. The solid lines are theories detailed in figure 6. Note that $\langle X^2 \rangle$ and D_x were obtained by fitting a single exponential relaxation to plots of $\langle X(t)X(t+\tau)\rangle$ versus the time lag τ: $\langle X^2 \rangle_0 \approx 584$ (a, right panel) and 511 (b, right panel) nm^2 and $D_0 \approx 0.25$ μm s^{-1}.

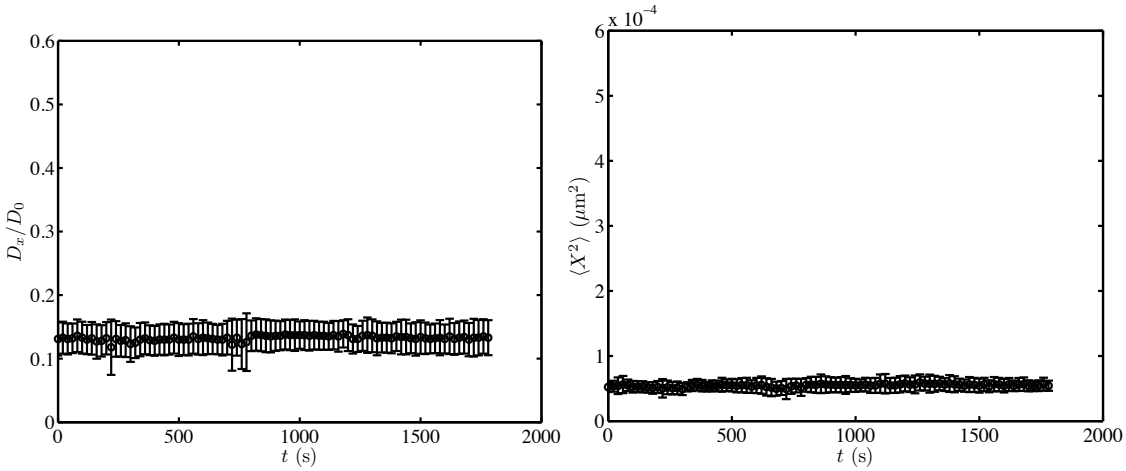

(a) DSPE-PEG2k-Amine/DOPC-coated silica microsphere on PA hydrogel A

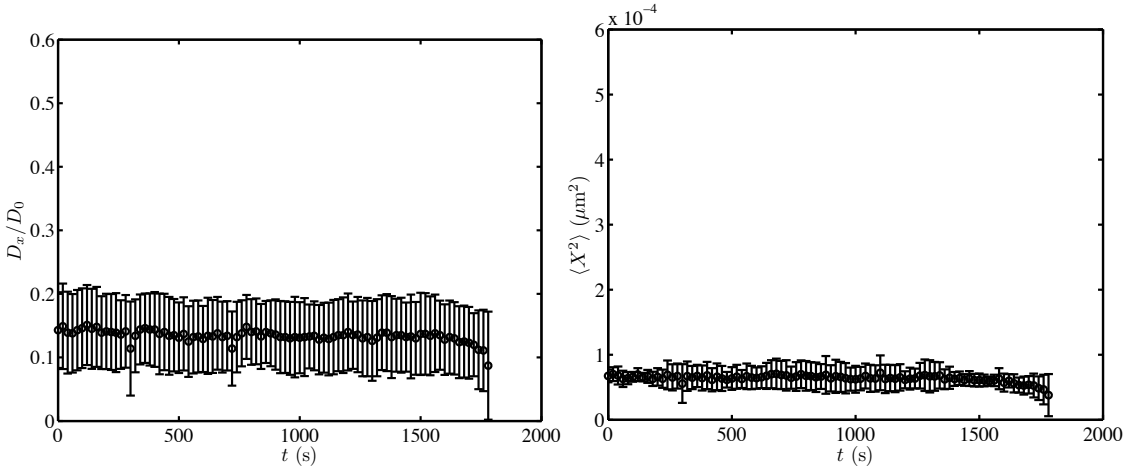

(b) DSPE-PEG2k-Amine/DOPC-coated silica microsphere on PA hydrogel B

Fig. 10 Average values of the short-time diffusion coefficient (left panel) and long-time Brownian position fluctuations variance (right panel) of DSPE-PEG2k-Amine (2.5 %)/DOPC-coated silica microspheres on PA gel A (panel a, with 7 particles) and B (panel b, with 3 particles). PEG chains firmly bind particles to the gel, as indicated by the lower diffusion coefficient and position variance. Compared to bare silica microspheres (figure 7), DSPE-PEG2k-Amine-coated particles adhere weakly, as indicated by a higher diffusion coefficient and position variance.

This journal is © The Royal Society of Chemistry [year]